

Geophysical Research Letters[®]



RESEARCH LETTER

10.1029/2024GL110362

Key Points:

- Electron advection and diffusion in wave-particle interactions with chorus waves are investigated through self-consistent simulations
- The second-order time derivative of gyrophase angle is nearly zero for phase-trapped electrons but is negative for phase-bunched electrons
- The advection and diffusion coefficients for cyclotron and Landau resonant electrons interacting with chorus waves are quantified

Supporting Information:

Supporting Information may be found in the online version of this article.

Correspondence to:

H. Chen and X. Wang,
huayue_chen@foxmail.com;
wangxue@auburn.edu

Citation:

Chen, H., Wang, X., Zhao, H., Lin, Y., Chen, L., Omura, Y., et al. (2024). Electron dynamics associated with advection and diffusion in self-consistent wave-particle interactions with oblique chorus waves. *Geophysical Research Letters*, 51, e2024GL110362. <https://doi.org/10.1029/2024GL110362>

Received 21 MAY 2024

Accepted 3 JUL 2024

Electron Dynamics Associated With Advection and Diffusion in Self-Consistent Wave-Particle Interactions With Oblique Chorus Waves

Huayue Chen¹ , Xueyi Wang¹ , Hong Zhao¹ , Yu Lin¹ , Lunjin Chen² , Yoshiharu Omura³ , Rui Chen¹ , and Yi-Kai Hsieh³

¹Department of Physics, Auburn University, Auburn, AL, USA, ²William B. Hanson Center for Space Sciences, University of Texas at Dallas, Richardson, TX, USA, ³Research Institute for Sustainable Humanosphere, Kyoto University, Kyoto, Japan

Abstract Chorus waves are intense electromagnetic emissions critical in modulating electron dynamics. In this study, we perform two-dimensional particle-in-cell simulations to investigate self-consistent wave-particle interactions with oblique chorus waves. We first analyze the electron dynamics sampled from cyclotron and Landau resonances with waves, and then quantify the advection and diffusion coefficients through statistical studies. It is found that phase-trapped cyclotron resonant electrons satisfy the second-order resonance condition and gain energy from waves. While phase-bunched cyclotron resonant electrons cannot remain in resonance for long periods. They transfer energy to waves and are scattered to smaller pitch angles. Landau resonant electrons are primarily energized by waves. For both types of resonances, advection coefficients are greater than diffusion coefficients when the wave amplitude is large. Our study highlights the important role of advection in electron dynamics modulation resulting from nonlinear wave-particle interactions.

Plain Language Summary Wave-particle interactions can modulate electron distributions through advection and diffusion. Previous studies focusing on advection and diffusion primarily relied on test particle simulations, which uses a simplified model of wave evolution. In this study, we perform self-consistent simulations to investigate the wave-particle interactions with chorus waves and quantify the advection and diffusion coefficients of resonant electrons. It is found that advection coefficients are greater than diffusion coefficients in both cyclotron and Landau resonances, indicating the significant role of nonlinear wave-particle interactions. The quantification of advection and diffusion coefficients in a self-consistent system is important for understanding and predicting the loss and energization processes in radiation belt electrons. This study complements previous diffusion models that regarded the evolution of electron dynamics in wave-particle interactions as a slow diffusive process.

1. Introduction

Chorus waves are intense and coherent electromagnetic emissions in the Earth's magnetosphere (Burtis & Helliwell, 1969; Chen, Wang, et al., 2023; Li et al., 2009; Tsurutani et al., 2009; Tsurutani & Smith, 1974), excited by the injections of \sim 10–100 keV electrons associated with substorms (Meredith et al., 2003; Li et al., 2009; Ma et al., 2022). These waves are scientifically interesting due to their crucial roles in modulating electron dynamics. For instance, they can scatter 10s of keV electrons into atmosphere, producing diffuse and pulsating auroras (Chen et al., 2020; Chen, Gao, et al., 2023; Gao et al., 2024; Zhao et al., 2021), and accelerate 100s of keV electrons to relativistic energies, forming the outer radiation belt (Foster et al., 2017; Omura et al., 2019; Thorne et al., 2013).

Wave-particle interactions can modify electron distributions through advection and diffusion (Albert & Bortnik, 2009; Artemyev et al., 2018; da Silva et al., 2018; Fu et al., 2019, 2020; Liu et al., 2012). Quasi-linear theory proposes that the distribution variations induced by chorus waves can be described in terms of diffusion, characterized by slow changes, assuming a constant wave spectrum and weak amplitude (Glauert & Horne, 2005; Kennel & Engelmann, 1966; Mourenas et al., 2012; Ni et al., 2014; Summers, 2005; Tu et al., 2013). While nonlinear theory suggests that advection is faster and more important than diffusion (Albert et al., 2021; Bortnik et al., 2008; Zhang et al., 2018). Therefore, how the variations resulting from both advection and diffusion caused

© 2024, The Author(s).

This is an open access article under the terms of the Creative Commons Attribution-NonCommercial-NoDerivs License, which permits use and distribution in any medium, provided the original work is properly cited, the use is non-commercial and no modifications or adaptations are made.

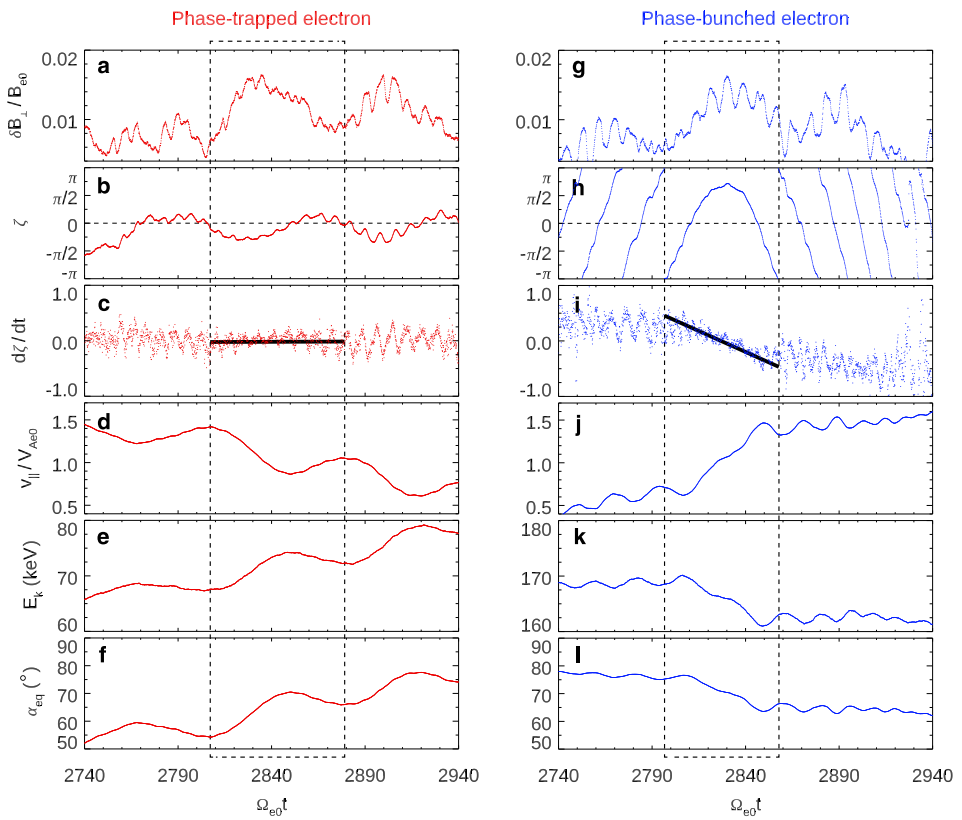


Figure 1. Temporal evolutions of (a, g) wave perpendicular magnetic field amplitude δB_\perp , (b, h) gyrophase angle ζ , (c, i) derivative $d\zeta/dt$, (d, j) parallel velocity v_\parallel , (e, k) kinetic energy E_k , and (f, l) equatorial pitch angle α_{eq} of electrons along their motion trajectories. The left (right) column in red (blue) is for the phase-trapped (phase-bunched) cyclotron resonant electron. The dashed boxes ($\Omega_{e0}t = 2,807\text{--}2,879$ in left column and $2,796\text{--}2,858$ in right column) mark the periods of ζ variation around T_s . The dotted lines in panels (b, h) indicate $\zeta = 0$. The thick black lines in panels (c, i) represent the linear fitting of $d^2\zeta/dt^2$.

by chorus waves affect electron precipitation and energization, and which type of variation is dominant, remain not fully understood.

Previous studies primarily relied on test particle simulations to calculate the advection and diffusion coefficients of particles under resonances with waves (Gan et al., 2020; Liu et al., 2012; Mourenas et al., 2012; Tao et al., 2012), where the spatiotemporal evolution of waves is pre-assumed. To fully address the physics in wave-particle interactions with oblique chorus waves, we perform self-consistent simulations and investigate the interactions through cyclotron and Landau resonances. Our findings reveal that the advection resulting from nonlinear effects plays a more significant role in modulating electron dynamics.

2. Simulation Model

We use a two-dimensional general curvilinear plasma simulation code (GCPIC) simulation model (Lu et al., 2019; Wang et al., 2024) in dipole fields to investigate the self-consistent wave-particle interactions. The reduced simulation domain is used, scaled to $L = 5.5\text{--}6.5$ with a scaling factor of 10. It covers a radial distance range from $p/(V_{Ae0}/\Omega_{e0}) = 1,511$ to 1,767 (where p represents the equatorial distance to the center of the Earth) and a latitude range from $\lambda \sim -30^\circ$ to $\sim 30^\circ$. Here, $V_{Ae0} = B_{e0}/\sqrt{\mu_0 n_{e0} m_e}$ is the electron Alfvén speed, $\Omega_{e0} = eB_{e0}/m_e$ is the equatorial electron gyrofrequency, μ_0 is the vacuum permeability, e and m_e are the charge and mass of an electron, B_{e0} is the background magnetic field at the equator, and n_{e0} is the plasma density. At the center of simulation domain, n_{e0} is 10 cm^{-3} and $B_{e0} = 144 \text{ nT}$. In this model, electrons are pushed by relativistic Lorentz force, and chorus waves are self-consistently excited by electrons with a temperature anisotropy. Other details of the model are available in Wang et al. (2024).

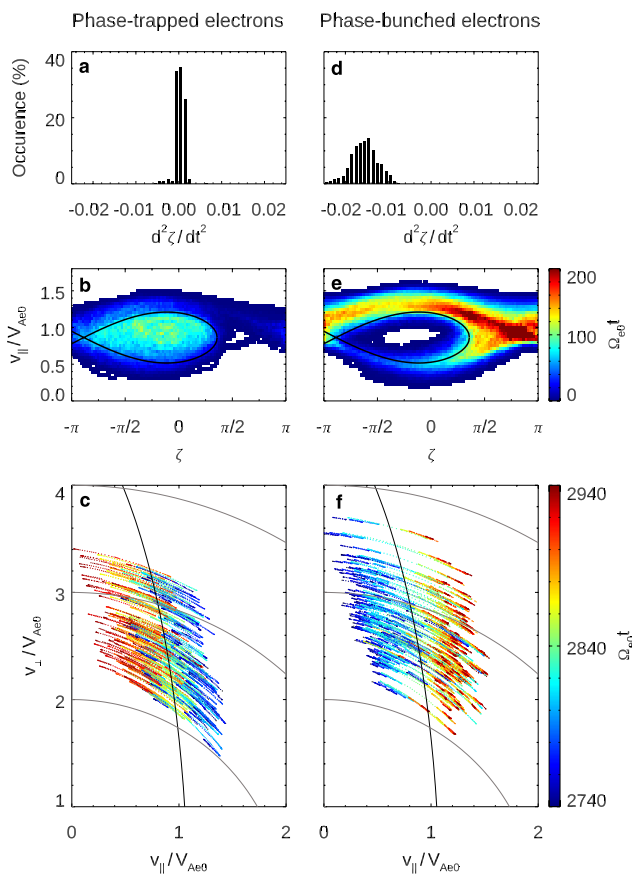


Figure 2. (a, d) Occurrence rates of $d^2\zeta/dt^2$, (b, e) dwell time in the $\zeta-v_{\parallel}$ planes, and (c, f) motion trajectories in the $v_{\parallel}-v_{\perp}$ planes. The left (right) column is for phase-trapped (phase-bunched) electrons. The black lines in panels (b, e) represent the envelope of the electron hole. In panels (c, f), the gray lines denote the contour lines of v_{\perp} , and the black lines represent the cyclotron resonance velocity v_c .

The dynamics of resonant electrons are studied using the retracing method (Chen et al., 2024). They are collected at a specific time point T_s and are analyzed from T_0 to T_f , with $T_0 < T_s < T_f$. These electrons are not treated as test particles; instead, they interact self-consistently with waves. In this study, we focus on the wave-particle interactions at $p/(V_{Ae0}/\Omega_{e0}) = 1,722$ and in the low latitude $\lambda = -7.6^\circ$, where chorus waves propagate obliquely against magnetic field lines with a wave normal angle of $\theta \sim 15^\circ$. The interactions through cyclotron and Landau resonances are separately investigated.

3. Simulation Results

3.1. Dynamics of Cyclotron Resonant Electrons

We first investigate the electron dynamics under cyclotron resonance with waves. At $\Omega_{e0}T_s = 2,840$, the cyclotron resonance velocity is calculated as $v_c = (\omega - \Omega_e/\gamma)/k_{\parallel} = 0.88V_{Ae0}$ (where $\Omega_e = eB_0/m_e$ is the local electron gyrofrequency, B_0 is the local background magnetic field, $\gamma = [1 - (v_{\parallel}^2 + v_{\perp}^2)/c^2]^{-1/2}$ is the Lorentz factor, v_{\parallel} and v_{\perp} are the parallel and perpendicular velocities, and c is the light speed), using a wave frequency of $\omega/\Omega_{e0} = 0.29$, a wave normal angle $\theta = 11.26^\circ$, and a wave number $kV_{Ae0}/\Omega_{e0} = -0.65$. Cyclotron resonant electrons are collected in the ranges of $v_{\parallel}/V_{Ae0} = 0.58-1.18$, $v_{\perp}/V_{Ae0} = 2-4$, and $\zeta = -\pi-\pi/2$, where ζ is the gyrophase angle between v_{\perp} and wave perpendicular magnetic field $\delta\mathbf{B}_{\perp}$. Cyclotron resonant electrons trapped in wave phases are categorized into phase-trapped and phase-bunched electrons (Albert et al., 2021; Chen et al., 2024; Liu et al., 2012; Matsumoto & Omura, 1981; Nunn, 1974). In this study, a total of 7,651 cyclotron resonant electrons are collected, comprising 2,288 phase-trapped electrons and 5,363 phase-bunched electrons. Their dynamics are investigated from $\Omega_{e0}T_0 = 2,740$ to $\Omega_{e0}T_f = 2,940$.

Figure 1 illustrates the examples of phase-trapped and phase-bunched electrons. The electrons move counter-stream to waves (Figure S1 in Supporting Information S1) and experience amplitude modulation during the traversal of wave packets (Figures 1a and 1g). Along their motion trajectories, the temporal evolutions of ζ for phase-trapped and phase-bunched electrons are different.

As shown in Figure 1b, the pattern of ζ evolution for the phase-trapped electron follows a sinusoidal function, with ζ confined within the range of $\zeta = -\pi/2-\pi/2$. Here, $\zeta = \pi/2$ denotes the positive direction of wave perpendicular electric field $\delta\mathbf{E}_{\perp}$ (refer to Figure S1 in Supporting Information S1 in Wang et al., 2024). When $\zeta < 0$, v_{\parallel} decreases due to the negative Lorentz force $dv_{\parallel}/dt = -ev_{\perp} \times \delta\mathbf{B}_{\perp}$, while E_k increases due to the positive energy transfer $-ev_{\perp} \cdot \delta\mathbf{E}_{\perp}$ (the terms $\delta\mathbf{E}_{\parallel}$ and $-ev_{\parallel} \cdot \delta\mathbf{E}_{\parallel}$ are significantly small and therefore neglected), resulting in an increase in α_{eq} . Conversely, v_{\parallel} increases but E_k and α_{eq} decrease when $\zeta > 0$. Within one ζ period (as indicated by the dashed box in Figure 1b), the electron spends more time at $\zeta < 0$, leading to the overall increase in E_k and α_{eq} (Figures 1e and 1f). Therefore, the phase-trapped electron gains energy from waves. For the phase-bunched electron, resonance interaction only occurs when v_{\parallel} is close to v_c during $\Omega_{e0}t = 2,796-2,858$ (marked by the dashed box in Figure 1j). As shown in Figure 1h, the pattern of ζ evolution follows a parabolic function in this interval, with ζ increasing from $-\pi$ to $\sim\pi/2$ and then returning to $-\pi$. Since the electron spends more time at $\zeta > 0$, E_k and α_{eq} exhibit an overall decrease (Figures 2k and 2l). Consequently, the phase-bunched electron transfers energy to waves.

For both phase-trapped and phase-bunched electrons, resonant interactions with waves correspond to $d\zeta/dt \sim 0$ (Figures 1c and 1i), which is the first-order resonance condition (Matsumoto & Omura, 1981; Vomvoridis et al., 1982). We then evaluate $d^2\zeta/dt^2$ by linearly fitting the slope of $d\zeta/dt$ (indicated by thick black lines) during resonant intervals. The $d^2\zeta/dt^2$ for the phase-trapped electron is nearly 0 with $d^2\zeta/dt^2 = 2.7 \times 10^{-4}$. While $d^2\zeta/dt^2 = -1.4 \times 10^{-2}$ is negative for the phase-bunched electron.

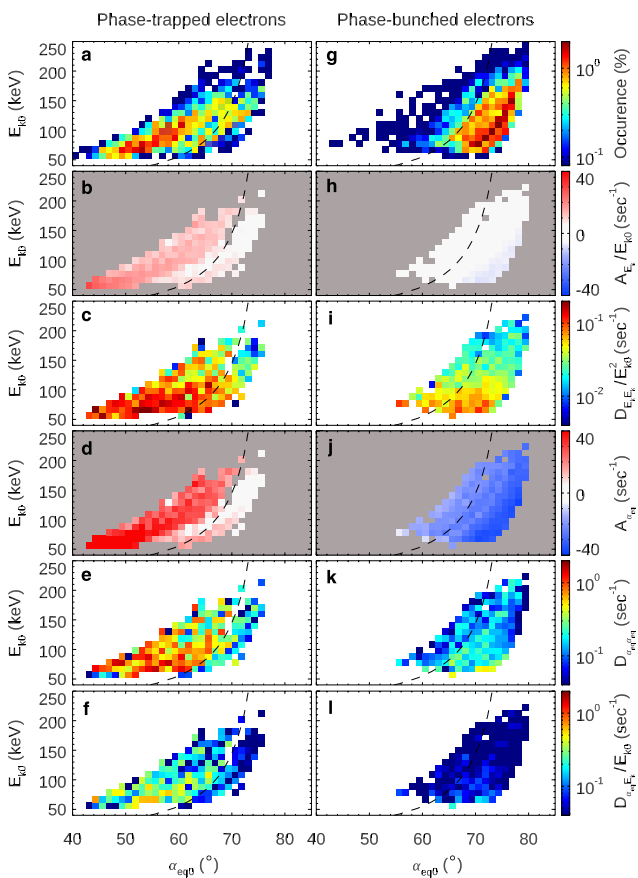


Figure 3. Distributions of (a, g) occurrence rate, (b, h) A_{E_k} , (c, i) $D_{E_kE_k}$, (d, j) $A_{\alpha_{eq}}$, (e, k) $D_{\alpha_{eq}\alpha_{eq}}$, and (f, l) $D_{\alpha_{eq}E_k}$ as a function of α_{eq0} and E_{k0} . The left (right) column is for phase-trapped (phase-bunched) electrons. The dashed line in each panel represents the cyclotron resonance line.

with color codes indicating temporal evolutions. For phase-trapped electrons, $v_{||}$ is larger than v_c at $\Omega_{e0}T_0 = 2,740$, but it decreases to the values smaller than v_c during resonance with waves. However, the total velocity $v_t = \sqrt{v_{||}^2 + v_{\perp}^2}$ (or E_k) increases since v_{\perp} grows significantly. In contrast, phase-bunched electrons exhibit $v_{||}$ smaller than v_c at T_0 , with $v_{||}$ increasing but v_t (or E_k) decreasing through the interaction. Due to the lower number density at larger $v_{||}$ in the Maxwellian distribution, an electron hole is formed when the phase-trapped electrons are inside the envelope (Figure 2b).

To quantify the variations of E_k and α_{eq} for phase-trapped and phase-bunched electrons, we calculate the advection and diffusion coefficients. Figure 3 illustrates the (a, g) occurrence rates of electrons at T_0 , (b, c, h, i) kinetic energy advection coefficient A_{E_k} and diffusion coefficient $D_{E_kE_k}$, (d, e, j, k) pitch angle advection coefficient $A_{\alpha_{eq}}$ and diffusion coefficient $D_{\alpha_{eq}\alpha_{eq}}$, and (f, l) cross diffusion coefficient $D_{\alpha_{eq}E_k}$ in the $\alpha_{eq0}-E_{k0}$ planes, where α_{eq0} and E_{k0} represent the α_{eq} and E_k values at T_0 . The occurrence rate is defined as the ratio of electron number in each bin to the total number of corresponding electrons. The black lines denote the cyclotron resonance energy as a function of equatorial pitch angle (referred to as cyclotron resonance line), estimated using the wave parameters at T_s . The coefficients are calculated by (Fu et al., 2020; Su et al., 2012; Zheng et al., 2012):

$$A_{E_k} = \frac{\langle E_{kf} - E_{k0} \rangle}{\Delta T}, \quad (2)$$

$$D_{E_kE_k} = \frac{\langle (E_{kf} - \langle E_{kf} \rangle)^2 \rangle}{2\Delta T}, \quad (3)$$

A statistical analysis of $d^2\zeta/dt^2$ is performed. Figures 2a and 2d shows the occurrence rate of $d^2\zeta/dt^2$, defined as the ratio between the number of electrons in each category and the total number of corresponding electrons. Phase-trapped electrons cluster around $d^2\zeta/dt^2 = 0$, satisfying the second-order resonance condition (Matsumoto & Omura, 1981; Vomvoridis et al., 1982), also known as “phase-locking” condition (Inan et al., 1978; Nunn, 1986; Tao et al., 2021). This indicates that phase-trapped electrons can maintain the resonant condition $d\zeta/dt \sim 0$ for the longest possible time, therefore maximizing the energy gain from waves. In contrast, phase-bunched electrons cannot remain in resonance for long periods due to negative $d^2\zeta/dt^2$, with the maximum occurrence rate at $d^2\zeta/dt^2 \sim -1.5 \times 10^{-2}$.

To further distinguish the two types of electrons, we present their distributions in the $\zeta-v_{||}$ planes in Figures 2b and 2e. The color codes indicate dwell time, which is statistically analyzed from $T_s - 20\Omega_{e0}^{-1}$ to $T_s + 20\Omega_{e0}^{-1}$. The black lines denote the envelope of the electron hole at T_s , defined as (Omura et al., 2008; Wang et al., 2024):

$$k^2(v_{||} - v_c)^2 + 2\omega_{ir}^2[\cos(\zeta + \pi) - S(\zeta + \pi)] = C, \quad (1)$$

where $\omega_{ir} = \omega_i\chi\gamma^{-1/2}$, $\omega_i = (k_{||}v_{\perp}e\delta B_{\perp}/m_e)^{1/2}$, $\chi = [1 - \omega^2/(k^2c^2)]^{1/2}$, S is the inhomogeneity factor, and C is a constant. At $\Omega_{e0}T_s = 2,840$, $\delta B_{\perp}/B_{e0} = 0.017$, S is -0.35 , and $v_{\perp}/V_{Ae0} = 2.5$. Phase-trapped electrons primarily localize inside the envelope, while phase-bunched electrons are outside and surround it. Moreover, phase-trapped electrons mainly cluster at $\zeta < 0$, corresponding to positive $-ev_{\perp} \cdot \delta E_{\perp}$ and energy gain from waves, whereas phase-bunched electrons concentrate at $\zeta > 0$, associated with negative $-ev_{\perp} \cdot \delta E_{\perp}$ and energy loss. Therefore, the tendency of energy variation revealed by statistical study is consistent with the results from single-particle analysis (Figure 1).

Additionally, the source of electrons in the velocity distribution is also different. Figures 2c and 2f illustrate electron trajectories in the $v_{||}-v_{\perp}$ planes,

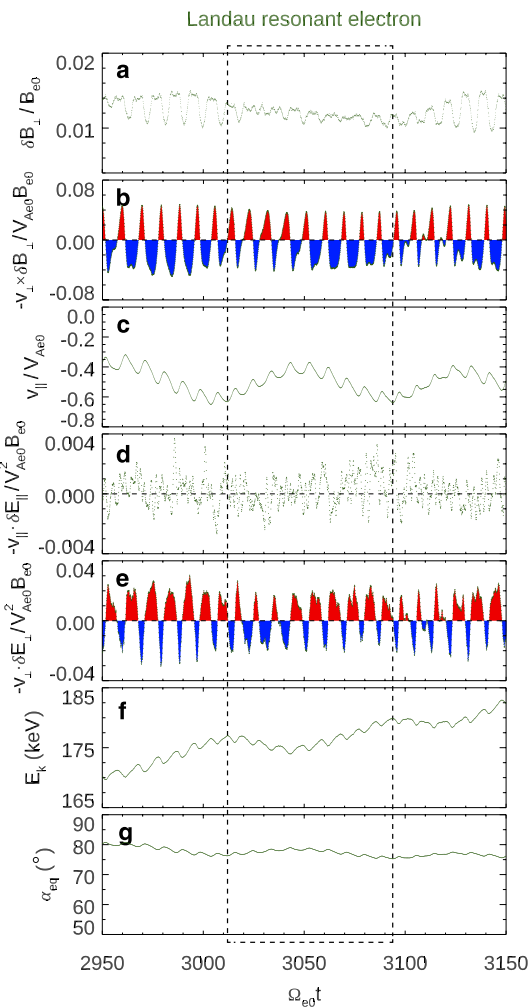


Figure 4. Temporal evolutions of (a) δB_\perp , (b) $-v_\perp \times \delta B_\perp$, (c) v_\parallel , (d) $-v_\perp \cdot \delta E_\parallel$, (e) $-v_\perp \cdot \delta E_\perp$, (f) E_k , and (g) α_{eq} of the Landau resonant electron along motion trajectory. The black dashed box marks the period of E_k variation around T_s . The dotted lines in panels (b, d, e) indicate the value 0. In panel (b), red (blue) color highlights the positive (negative) values of $-v_\perp \times \delta B_\perp$ or $-v_\perp \cdot \delta E_\perp$.

$$A_{\alpha_{eq}} = \frac{\langle \alpha_{eqf} - \alpha_{eq0} \rangle}{\Delta T}, \quad (4)$$

$$D_{\alpha_{eq}\alpha_{eq}} = \frac{\langle (\alpha_{eqf} - \langle \alpha_{eqf} \rangle)^2 \rangle}{2\Delta T}, \quad (5)$$

$$D_{\alpha_{eq}E_k} = \frac{\langle (\alpha_{eqf} - \langle \alpha_{eqf} \rangle)(E_{kf} - \langle E_{kf} \rangle) \rangle}{2\Delta T}, \quad (6)$$

where α_{eqf} and E_{kf} represent the values at T_f , ΔT is the interval of $200 \Omega_{e0}^{-1}$, and $\langle \dots \rangle$ denotes averaging over all electrons. To reduce statistical errors, only the coefficients with occurrence rates above 0.1% are presented. In this study, cyclotron resonant electrons are investigated in the ranges of $\alpha_{eq0} = 40^\circ\text{--}80^\circ$ and $E_{k0} = 50\text{--}250$ keV, clustering around the cyclotron resonance line. Phase-trapped electrons mainly fall in the range of $E_{k0} = 50\text{--}200$ keV, and their $\alpha_{eq0} = 46^\circ\text{--}64^\circ$ are smaller than those on the cyclotron resonance line (Figure 3a). While phase-bunched electrons primarily correspond to larger $\alpha_{eq0} = 66^\circ\text{--}78^\circ$ (Figure 3g), consistent with their smaller v_\parallel at T_0 (Figure 2f). For both types of electrons, advection coefficients are two orders of magnitude larger than diffusion coefficients, indicating the significant role of nonlinear wave-particle interaction through cyclotron resonance. Moreover, α_{eq} advection is more efficient than E_k advection. Specifically, phase-trapped electrons exhibit positive E_k and α_{eq} advectives, with mean values of $A_{E_k}/E_{k0} \sim 10 \text{ s}^{-1}$ and $A_{\alpha_{eq}} \sim 20 \text{ s}^{-1}$, especially for the electrons with smaller α_{eq0} (Figures 3b and 3d). These electrons are energized due to energy gain from waves. In contrast, phase-bunched electrons with larger α_{eq0} show weaker and negative E_k advection with mean $A_{E_k}/E_{k0} \sim -5 \text{ s}^{-1}$ (Figure 3h), transferring energy to waves. They are also scattered to smaller pitch angles due to negative α_{eq} advection with mean $A_{\alpha_{eq}} \sim -25 \text{ s}^{-1}$ (Figure 3j).

3.2. Dynamics of Landau Resonant Electrons

We then investigate the dynamics of Landau resonant electrons, which are collected at $\Omega_{e0}T_s = 3,050$. The wave frequency, wave normal angle, and wave number are $\omega/\Omega_{e0} = 0.36$, $\theta = 13.38^\circ$ and $kV_{Ae0}/\Omega_{e0} = -0.76$, respectively, leading to the Landau resonance velocity of $v_L = \omega/k = -0.48V_{Ae0}$. The electrons are collected in the ranges of $v_\parallel/V_{Ae0} = -0.78\text{--}0.18$, $v_\perp/V_{Ae0} = 2\text{--}4$, and $\zeta = -\pi\text{--}\pi/2$. There are a total of 6,069 Landau resonant electrons, and their dynamics are investigated from $\Omega_{e0}T_0 = 2,950$ to $\Omega_{e0}T_f = 3,150$.

Figure 4 presents a typical example. The Landau resonant electron moves co-stream with wave packets (Figure S1 in Supporting Information S1), experiencing nearly constant wave phases and amplitudes ($\delta B_\perp/B_{e0} \sim 0.013$, as shown in Figure 4a). During each gyroperiod (lasting approximately $9 \Omega_{e0}^{-1}$), there is energy transfer between waves and particles, with a nonzero net energy transfer due to the finite perpendicular wave number k_\perp (Chen & Bortnik, 2020; Omura et al., 2019). As depicted in Figures 4b and 4c, the temporal variation of v_\parallel is determined by $-ev_\perp \times \delta B_\perp$, with $|v_\parallel|$ decreasing (increasing) at positive (negative) $-ev_\perp \times \delta B_\perp$. The δE_\parallel term in the Lorentz force is significantly small and therefore neglected (not shown). The E_k variation is determined by $-ev_\perp \cdot \delta E_\perp$ rather than $-ev_\parallel \cdot \delta E_\parallel$ (Figure 4f, the details are in the Supporting Information S1), where $-ev_\perp \cdot \delta E_\perp$ is one order of magnitude larger than $-ev_\parallel \cdot \delta E_\parallel$ (Figures 4d and 4e). This is a typical characteristic of electromagnetic Landau resonance (Hsieh & Omura, 2018; Liu et al., 2024; Omura et al., 2019). In Figures 4b and 4e, red (blue) color highlights the positive (negative) values of $-ev_\perp \times \delta B_\perp$ and $-ev_\perp \cdot \delta E_\perp$. During intervals with positive net $-ev_\perp \times \delta B_\perp$ and negative net $-ev_\perp \cdot \delta E_\perp$ (e.g., $\Omega_{e0}t = 3,012\text{--}3,042$), both $|v_\parallel|$ and E_k decrease. Meanwhile, v_\perp remains almost unchanged during resonance, resulting in an increase in α_{eq} (Figure 4g). Conversely, during intervals with negative net $-ev_\perp \times \delta B_\perp$ and positive net $-ev_\perp \cdot \delta E_\perp$ (e.g., $\Omega_{e0}t = 3,042\text{--}3,093$), $|v_\parallel|$ and E_k increase

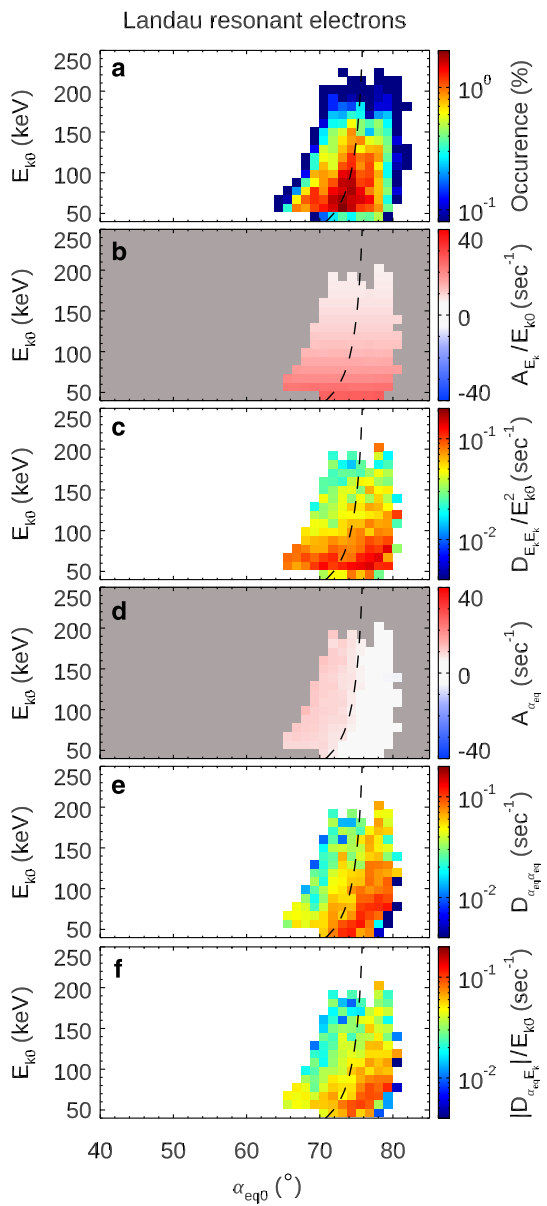


Figure 5. (a) Occurrence rate and (b–f) advection and diffusion coefficients in the α_{eq0} – E_{k0} planes for Landau resonant electrons, following the format of Figure 3. The dashed line in each panel represents the Landau resonance line. Since α_{eq} and E_k of Landau resonant electrons exhibit opposite variations, the absolute values of $D_{\alpha_{eq}E_k}$ are presented in panel (f).

~ 0.05 – 0.1 s⁻¹ and $D_{\alpha_{eq}\alpha_{eq}}$ to be ~ 0.5 – 1.0 s⁻¹ along the cyclotron resonance line. These estimations match the diffusion coefficients derived from particle dynamics (Figures 3c and 3e). Note that in our simulations, $D_{E_kE_k}/E_{k0}^2$ and $D_{\alpha_{eq}\alpha_{eq}}$ are two orders of magnitude larger than those in observations (Mourenas et al., 2012; Ni et al., 2014; Tao et al., 2012; Tu et al., 2013). This discrepancy arises from the reduced simulation domain, where wave amplitude δB is one order of magnitude larger than observational values (Ma et al., 2022), resulting in a two-order-of-magnitude amplification of diffusion coefficients as they are proportional to δB^2 (Liu et al., 2010). Besides, the calculation of diffusion coefficients in observations generally relies on stable wave models, which only consider the energy transfer from waves to particles. In this work, we use a self-consistent model, where waves are excited by particles, considering both the energy transfers from waves to particles and the feedback

but α_{eq} decreases. The period of E_k variation around T_s is indicated by the black dashed box from $\Omega_{eq0}t = 3,012$ to $3,093$, established via the adjacent maximum E_k values. Within one period, the net energy transfer predominantly occurs from waves to particles, leading to an overall increase in $|\mathbf{v}_{\parallel}|$ and E_k . The electron gains energy from chorus waves.

We further calculate the advection and diffusion coefficients for Landau resonant electrons based on Equations 2–6. Here, α_{eq0} and E_{k0} (α_{eqf} and E_{kf}) represent the values at T_0 (T_f), and only the coefficients with occurrence rates above 0.1% are presented. The dashed lines represent the Landau resonance energy as a function of equatorial pitch angle (referred to as Landau resonance line), estimated using the wave parameters at T_s . The electrons cluster around the Landau resonance line in the ranges of $\alpha_{eq0} = 65^\circ$ – 80° and $E_{k0} = 40$ – 230 keV (Figure 5a). As shown in Figures 5b–5f, the advection coefficients are two orders of magnitude larger than diffusion coefficients, indicating that nonlinear effects also dominate the wave-particle interaction through Landau resonance. Furthermore, E_k advection is more efficient than α_{eq} advection. The electrons in the lower energy range of $E_{k0} = 40$ – 100 keV exhibit strong E_k advection with the mean value of $A_{E_k}/E_{k0} \sim 10$ s⁻¹ (Figure 5b), and those with smaller α_{eq0} correspond to a weak increase in α_{eq} with $A_{\alpha_{eq}}$ of ~ 7 s⁻¹ (Figure 5d). Therefore, Landau resonant electrons are primarily energized by chorus waves. Additionally, energization through Landau resonance can be more efficient than through cyclotron resonance due to the longer interaction time, as Landau resonant electrons move co-stream with wave packets (Omura et al., 2019).

4. Summary and Discussions

In this study, we investigate electron dynamics through cyclotron and Landau resonances with oblique chorus waves and quantify the advection and diffusion coefficients in self-consistent wave-particle interactions. For both kinds of resonances, advection coefficients are greater than diffusion coefficients when the wave amplitude is large. Phase-trapped cyclotron resonant electrons satisfy the phase-locking condition $d^2\zeta/dt^2 \sim 0$, enabling them to maintain resonance with waves. They are mainly in the ranges of $\alpha_{eq} = 46^\circ$ – 64° and $E_k = 50$ – 200 keV, exhibiting positive α_{eq} and E_k advects and gaining energies from waves. On the other hand, phase-bunched electrons, which concentrate in $\alpha_{eq0} = 66^\circ$ – 78° and $E_k = 50$ – 200 keV, cannot remain in resonance for long periods due to $d^2\zeta/dt^2 < 0$. They are characterized by negative α_{eq} and E_k advects, transferring energies to waves and being scattered to smaller pitch angles. Landau resonant electrons primarily fall within $\alpha_{eq} = 65^\circ$ – 80° and $E_k = 40$ – 100 keV and are energized with positive E_k advection.

By integrating simulated wave parameters into quasi-linear theory models (Glauert & Horne, 2005; Summers, 2005), we estimate $D_{E_kE_k}/E_{k0}^2$ to be

from particles to waves. Further investigation will focus on clarifying the relation between advection/diffusion coefficients and wave amplitude through parametric studies.

The quantification of advection and diffusion coefficients in self-consistent wave-particle interactions is crucial for understanding and predicting the loss and energization processes in radiation belt electrons. Our study highlights the significant roles of advection and associated nonlinear wave-particle interactions, providing an important complement to previous diffusion models. In this study, we mainly focus on the wave-particle interactions in lower latitudes. The physics in higher latitudes, where chorus waves may turn highly oblique, is also interesting and important. We leave this for future work. To verify the influence of advection and diffusion coefficients on electron dynamics, we need to perform electron dynamic simulations (e.g., Fokker-Plank equation simulation) and compare the results with satellite observations. It is our next target and will be addressed in subsequent work.

Data Availability Statement

The simulation data are available in Chen (2024).

Acknowledgments

This work was supported by the NASA Grants 80NSSC24K0174, 80NSSC21K1688, 80NSSC21K1679, 80NSSC20K1322, 80NSSC23K0086, 80NSSC22K1012, and the NSF Grants AGS-2131012, AGS-2247759, and AGS-2224109. HZ was supported by the NASA Grant 80NSSC22K0473. LC was supported by the NASA Grant 80NSSC24K0174, the AFOSR grant of FA9550-23-1-0568, and the NSF grant AGS-2225121. YO and YH were supported by JSPS KAKENHI Grant JP24K00691 and JP23H05429. Computer resources are provided by NASA NAS Division.

References

- Albert, J. M., Artemyev, A. V., Li, W., Gan, L., & Ma, Q. (2021). Models of resonant wave-particle interactions. *Journal of Geophysical Research: Space Physics*, 126(6), e2021JA029216. <https://doi.org/10.1029/2021JA029216>
- Albert, J. M., & Bortnik, J. (2009). Nonlinear interaction of radiation belt electrons with electromagnetic ion cyclotron waves. *Geophysical Research Letters*, 36(12). <https://doi.org/10.1029/2009GL038904>
- Artemyev, A. V., Neishtadt, A. I., Vasiliev, A. A., & Mourenas, D. (2018). Long-term evolution of electron distribution function due to nonlinear resonant interaction with whistler mode waves. *Journal of Plasma Physics*, 84(2), 905840. <https://doi.org/10.1017/S0022377818000260>
- Bortnik, J., Thorne, R. M., & Inan, U. S. (2008). Nonlinear interaction of energetic electrons with large amplitude chorus. *Geophysical Research Letters*, 35(21), L21102. <https://doi.org/10.1029/2008GL035500>
- Burtis, W. J., & Helliwell, R. A. (1969). Banded chorus a new type of VLF radiation observed in the magnetosphere by OGO 1 and OGO 3. *Journal of Geophysical Research*, 74(11), 3002–3010. <https://doi.org/10.1029/JA074i011p03002>
- Chen, H. (2024). Database of electron dynamics in self-consistent wave-particle interactions with oblique chorus waves [Dataset]. Zenodo. <https://doi.org/10.5281/zenodo.1099344>
- Chen, H., Gao, X., Lu, Q., & Tsurutani, B. T. (2023). Global distribution of relativistic electron precipitation and the dependences on substorm injection and solar wind ram pressure: Long-term POES observations. *Journal of Geophysical Research: Space Physics*, 128(11), e2023JA031566. <https://doi.org/10.1029/2023JA031566>
- Chen, H., Wang, X., Chen, L., Omura, Y., Tsurutani, B. T., Lin, Y., & Xia, Z. (2023). Evolution of chorus subpackets in the Earth's magnetosphere. *Geophysical Research Letters*, 50(21), e2023GL105938. <https://doi.org/10.1029/2023GL105938>
- Chen, H., Wang, X., Chen, L., Zhang, X., Omura, Y., Chen, R., et al. (2024). Nonlinear electron trapping through cyclotron resonance in the formation of chorus subpackets. *Geophysical Research Letters*, 51(11), e2024GL109481. <https://doi.org/10.1029/2024GL109481>
- Chen, L., & Bortnik, J. (2020). Chapter 4-Wave-particle interactions with coherent magnetosonic waves. In A. N. Jaynes & M. E. Usanova (Eds.), *The dynamic loss of Earth's radiation belts* (pp. 99–120). Elsevier. <https://doi.org/10.1016/B978-0-12-813371-2.00004-4>
- Chen, L., Breneman, A. W., Xia, Z., & Zhang, X.-J. (2020). Modeling of bouncing electron microbursts induced by ducted chorus waves. *Geophysical Research Letters*, 47(17), e2020GL089400. <https://doi.org/10.1029/2020GL089400>
- da Silva, C. L., Denton, R. E., Hudson, M. K., Millan, R. M., Liu, K., & Bortnik, J. (2018). Test-particle simulations of linear and nonlinear interactions between a 2-D whistler-mode wave packet and radiation belt electrons. *Geophysical Research Letters*, 45(11), 5234–5245. <https://doi.org/10.1029/2018GL077877>
- Foster, J. C., Erickson, P. J., Omura, Y., Baker, D. N., Kletzing, C. A., & Claudepierre, S. G. (2017). Van Allen Probes observations of prompt MeV radiation belt electron acceleration in nonlinear interactions with VLF chorus. *Journal of Geophysical Research: Space Physics*, 122(1), 324–339. <https://doi.org/10.1002/2016JA023429>
- Fu, S., Ni, B., Zhou, R., Cao, X., & Gu, X. (2019). Combined scattering of radiation belt electrons caused by Landau and bounce resonant interactions with magnetosonic waves. *Geophysical Research Letters*, 46(17–18), 10313–10321. <https://doi.org/10.1029/2019GL084438>
- Fu, S., Yi, J., Ni, B., Zhou, R., Hu, Z., Cao, X., et al. (2020). Combined scattering of radiation belt electrons by low-frequency hiss: Cyclotron, Landau, and bounce resonances. *Geophysical Research Letters*, 47(5), e2020GL086963. <https://doi.org/10.1029/2020GL086963>
- Gan, L., Li, W., Ma, Q., Albert, J. M., Artemyev, A. V., & Bortnik, J. (2020). Nonlinear interactions between radiation belt electrons and chorus waves: Dependence on wave amplitude modulation. *Geophysical Research Letters*, 47(4), e2019GL085987. <https://doi.org/10.1029/2019GL085987>
- Gao, X., Ma, J., Shao, T., Chen, R., Ke, Y., & Lu, Q. (2024). Why chorus waves are the dominant driver for diffuse auroral precipitation. *Science Bulletin*, 69, 5–600. <https://doi.org/10.1016/j.scib.2023.12.009>
- Glauert, S. A., & Horne, R. B. (2005). Calculation of pitch angle and energy diffusion coefficients with the PADIE code. *Journal of Geophysical Research*, 110(A4), A04206. <https://doi.org/10.1029/2004JA010851>
- Hsieh, Y.-K., & Omura, Y. (2018). Nonlinear damping of oblique whistler mode waves via Landau resonance. *Journal of Geophysical Research: Space Physics*, 123(9), 7462–7472. <https://doi.org/10.1029/2018JA025848>
- Inan, U. S., Bell, T. F., & Helliwell, R. A. (1978). Nonlinear pitch angle scattering of energetic electrons by coherent VLF waves in the magnetosphere. *Journal of Geophysical Research*, 83(A7), 3235–3253. <https://doi.org/10.1029/JA083iA07p03235>
- Kennel, C. F., & Engelmann, F. (1966). Velocity space diffusion from weak plasma turbulence in a magnetic field. *The Physics of Fluids*, 9(12), 2377–2388. <https://doi.org/10.1063/1.1761629>
- Li, W., Thorne, R. M., Angelopoulos, V., Bortnik, J., Cully, C. M., Ni, B., et al. (2009). Global distribution of whistler-mode chorus waves observed on the THEMIS spacecraft. *Geophysical Research Letters*, 36(9), L09104. <https://doi.org/10.1029/2009GL037595>

- Liu, K., Lemons, D. S., Winske, D., & Gary, S. P. (2010). Relativistic electron scattering by electromagnetic ion cyclotron fluctuations: Test particle simulations. *Journal of Geophysical Research*, 115(A4), A04204. <https://doi.org/10.1029/2009JA014807>
- Liu, K., Winske, D., Gary, S. P., & Reeves, G. D. (2012). Relativistic electron scattering by large amplitude electromagnetic ion cyclotron waves: The role of phase bunching and trapping. *Journal of Geophysical Research*, 117(A6). <https://doi.org/10.1029/2011JA017476>
- Liu, Z.-Y., Zong, Q.-G., Wang, Y.-F., Zhou, X.-Z., Wang, S., & Li, J.-H. (2024). Electromagnetic Landau resonance: MMS observations. *Geophysical Research Letters*, 51(6), e2023GL105734. <https://doi.org/10.1029/2023GL105734>
- Lu, Q., Ke, Y., Wang, X., Liu, K., Gao, X., Chen, L., & Wang, S. (2019). Two-dimensional general curvilinear particle-in-cell (gcPIC) simulation of rising-tone chorus waves in a dipole magnetic field. *Journal of Geophysical Research: Space Physics*, 124(6), 4157–4167. <https://doi.org/10.1029/2019JA026586>
- Ma, J., Gao, X., Chen, H., Tsurutani, B. T., Ke, Y., Chen, R., & Lu, Q. (2022). The effects of substorm injection of energetic electrons and enhanced solar wind ram pressure on whistler-mode chorus waves: A statistical study. *Journal of Geophysical Research: Space Physics*, 127(11), e2022JA030502. <https://doi.org/10.1029/2022JA030502>
- Matsumoto, H., & Omura, Y. (1981). Cluster and channel effect phase bunchings by whistler waves in the nonuniform geomagnetic field. *Journal of Geophysical Research*, 86(A2), 779–791. <https://doi.org/10.1029/JA086iA02p00779>
- Meredith, N. P., Horne, R. B., Thorne, R. M., & Anderson, R. R. (2003). Favored regions for chorus-driven electron acceleration to relativistic energies in the Earth's outer radiation belt. *Geophysical Research Letters*, 30(16), 1871. <https://doi.org/10.1029/2003GL017698>
- Mourenas, D., Artemyev, A. V., Ripoll, J.-F., Agapitov, O. V., & Krasnoselskikh, V. V. (2012). Timescales for electron quasi-linear diffusion by parallel and oblique lower-band chorus waves. *Journal of Geophysical Research*, 117(A6), A06234. <https://doi.org/10.1029/2012JA017717>
- Ni, B., Bortnik, J., Nishimura, Y., Thorne, R. M., Li, W., Angelopoulos, V., et al. (2014). Chorus wave scattering responsible for the Earth's dayside diffuse auroral precipitation: A detailed case study. *Journal of Geophysical Research: Space Physics*, 119(2), 897–908. <https://doi.org/10.1002/2013JA019507>
- Nunn, D. (1974). A self-consistent theory of triggered VLF emissions. *Planetary and Space Science*, 22(3), 349–378. [https://doi.org/10.1016/0032-0633\(74\)90070-1](https://doi.org/10.1016/0032-0633(74)90070-1)
- Nunn, D. (1986). A nonlinear theory of sideband stability in ducted whistler mode waves. *Planetary and Space Science*, 34(5), 429–451. [https://doi.org/10.1016/0032-0633\(86\)90032-2](https://doi.org/10.1016/0032-0633(86)90032-2)
- Omura, Y., Hsieh, Y.-K., Foster, J. C., Erickson, P. J., Kletzing, C. A., & Baker, D. N. (2019). Cyclotron acceleration of relativistic electrons through Landau resonance with obliquely propagating whistler-mode chorus emissions. *Journal of Geophysical Research: Space Physics*, 124(4), 2795–2810. <https://doi.org/10.1029/2018JA026374>
- Omura, Y., Katoh, Y., & Summers, D. (2008). Theory and simulation of the generation of whistler-mode chorus. *Journal of Geophysical Research*, 113(A4), A04223. <https://doi.org/10.1029/2007JA012622>
- Su, Z., Zhu, H., Xiao, F., Zheng, H., Shen, C., Wang, Y., & Wang, S. (2012). Bounce-averaged advection and diffusion coefficients for monochromatic electromagnetic ion cyclotron wave: Comparison between test-particle and quasi-linear models. *Journal of Geophysical Research*, 117(A9), A09222. <https://doi.org/10.1029/2012JA017917>
- Summers, D. (2005). Quasi-linear diffusion coefficients for field-aligned electromagnetic waves with applications to the magnetosphere. *Journal of Geophysical Research*, 110(A8), A08213. <https://doi.org/10.1029/2005JA011159>
- Tao, X., Bortnik, J., Albert, J. M., & Thorne, R. M. (2012). Comparison of bounce-averaged quasi-linear diffusion coefficients for parallel propagating whistler mode waves with test particle simulations. *Journal of Geophysical Research*, 117(A10), A10205. <https://doi.org/10.1029/2012JA017931>
- Tao, X., Zonca, F., & Chen, L. (2021). A “Trap-Release-Amplify” model of chorus waves. *Journal of Geophysical Research: Space Physics*, 126(9), e2021JA029585. <https://doi.org/10.1029/2021JA029585>
- Thorne, R. M., Li, W., Ni, B., Ma, Q., Bortnik, J., Chen, L., et al. (2013). Rapid local acceleration of relativistic radiation-belt electrons by magnetospheric chorus. *Nature*, 504(7480), 411–414. <https://doi.org/10.1038/nature12889>
- Tsurutani, B. T., & Smith, E. J. (1974). Postmidnight chorus: A substorm phenomenon. *Journal of Geophysical Research*, 79(1), 118–127. <https://doi.org/10.1029/JA079i001p00118>
- Tsurutani, B. T., Verkhoglyadova, O. P., Lakhina, G. S., & Yagitani, S. (2009). Properties of dayside outer zone chorus during HILDCAA events: Loss of energetic electrons. *Journal of Geophysical Research*, 114(A3), A03207. <https://doi.org/10.1029/2008JA013353>
- Tu, W., Cunningham, G. S., Chen, Y., Henderson, M. G., Camporeale, E., & Reeves, G. D. (2013). Modeling radiation belt electron dynamics during GEM challenge intervals with the DREAM3D diffusion model. *Journal of Geophysical Research: Space Physics*, 118(10), 6197–6211. <https://doi.org/10.1002/jgra.50560>
- Vomvoridis, J. L., Crystal, T. L., & Denavit, J. (1982). Theory and computer simulations of magnetospheric very low frequency emissions. *Journal of Geophysical Research*, 87(A3), 1473–1489. <https://doi.org/10.1029/JA087iA03p01473>
- Wang, X., Chen, H., Omura, Y., Hsieh, C. L., Lin, Y., Zhang, X.-J., & Xia, Z. (2024). Resonant electron signatures in the formation of chorus wave subpackets. *Geophysical Research Letters*, 51(8). <https://doi.org/10.1029/2023GL108000>
- Zhang, X.-J., Thorne, R., Artemyev, A., Mourenas, D., Angelopoulos, V., Bortnik, J., et al. (2018). Properties of intense field-aligned lower-band chorus waves: Implications for nonlinear wave-particle interactions. *Journal of Geophysical Research: Space Physics*, 123(7), 5379–5393. <https://doi.org/10.1029/2018JA025390>
- Zhao, H., Friedel, R. H. W., Chen, Y., Baker, D. N., Li, X., Malaspina, D. M., et al. (2021). Equatorial pitch angle distributions of 1–50 keV electrons in Earth's inner magnetosphere: An empirical model based on the Van Allen Probes observations. *Journal of Geophysical Research: Space Physics*, 126(1), e2020JA028322. <https://doi.org/10.1029/2020JA028322>
- Zheng, Q., Zheng, Y., Fok, M.-C., & Lui, A. T. (2012). Electron energy diffusion and advection due to non-linear electron-chorus wave interactions. *Journal of Atmospheric and Solar-Terrestrial Physics*, 80, 152–160. <https://doi.org/10.1016/j.jastp.2012.01.011>